Human Molecular Genetics, 2011, Vol. 20, No. 23 **4582–4596**
doi:10.1093/hmg/ddr392
Advance Access published on August 31, 2011

Restrictive loss of plakoglobin in cardiomyocytes leads to arrhythmogenic cardiomyopathy

Deqiang Li[1,2], Ying Liu[2,3], Mitsunori Maruyama[4], Wuqiang Zhu[1,2], Hanying Chen[1,2], Wenjun Zhang[1,2], Sean Reuter[1,2], Shien-Fong Lin[4], Laura S. Haneline[2,3], Loren J. Field[1,2,4], Peng-Sheng Chen[4] and Weinian Shou[1,2,*]

[1]Riley Heart Research Center, [2]Herman B Wells Center for Pediatric Research, Department of Pediatrics, [3]Department of Microbiology and Immunology and [4]The Krannert Institute of Cardiology and the Division of Cardiology, Indiana University School of Medicine, Indianapolis, IN 46202, USA

Received June 12, 2011; Revised August 19, 2011; Accepted August 28, 2011

Arrhythmogenic right ventricular cardiomyopathy (ARVC) is an inheritable myocardial disorder associated with fibrofatty replacement of myocardium and ventricular arrhythmia. A subset of ARVC is categorized as Naxos disease, which is characterized by ARVC and a cutaneous disorder. A homozygous loss-of-function mutation of the Plakoglobin (Jup) gene, which encodes a major component of the desmosome and the adherens junction, had been identified in Naxos patients, although the underlying mechanism remained elusive. We generated *Jup* mutant mice by ablating *Jup* in cardiomyocytes. *Jup* mutant mice largely recapitulated the clinical manifestation of human ARVC: ventricular dilation and aneurysm, cardiac fibrosis, cardiac dysfunction and spontaneous ventricular arrhythmias. Ultra-structural analyses revealed that desmosomes were absent in *Jup* mutant myocardia, whereas adherens junctions and gap junctions were preserved. We found that ventricular arrhythmias were associated with progressive cardiomyopathy and fibrosis in *Jup* mutant hearts. Massive cell death contributed to the cardiomyocyte dropout in *Jup* mutant hearts. Despite the increase of β-catenin at adherens junctions in *Jup* mutant cardiomyoicytes, the Wnt/β-catenin-mediated signaling was not altered. Transforming growth factor-beta-mediated signaling was found significantly elevated in *Jup* mutant cardiomyocytes at the early stage of cardiomyopathy, suggesting an important pathogenic pathway for Jup-related ARVC. These findings have provided further insights for the pathogenesis of ARVC and potential therapeutic interventions.

INTRODUCTION

Arrhythmogenic right ventricular cardiomyopathy (ARVC), also referred to as arrhythmogenic right ventricular dysplasia (ARVD), is an inheritable myocardial disorder associated with fibrofatty replacement of myocardium, ventricular arrhythmia and sudden death. The typical form of ARVC predominantly hits the right ventricle (RV) at early stage and affects the left ventricle (LV) with disease progression, although the recent wide recognition of left and biventricular subtypes has broadened the definition of ARVC (1). The incidence of ARVC has been reported to be ∼1/10 000 in the general population in the United States (2). It also accounts for up to 10% of unexplained sudden cardiac deaths in individuals <65 years old (3). A subset of ARVC is categorized as Naxos disease, which is characterized by ARVC and a cutaneous disorder. In contrast to an autosomal-dominant inheritance pattern as seen in most other ARVC patients, Naxos disease exhibits an autosomal-recessive pattern of inheritance (4).

Mutations in multiple genes including Desmoplakin, Desmoglein 2, Desmocollin 2, Plakophilin 2, Plakoglobin (Jup, also called γ-catenin), Ryanodine receptor 2, Laminin receptor 1 and transforming growth factor-beta 3 (TGFβ3) have been identified in ARVC patients (2,5,6). The heterogeneity of genetic mutations in ARVC patients underscores the complexity of the pathogenesis. Notably, many of these genetic mutations identified in ARVC

*To whom correspondence should be addressed at: Herman B Wells Center for Pediatric Research. R4-302D, 1044 West Walnut, Indianapolis, IN 46202, USA. Tel: +1 3172748952; Fax: +1 3172789298; Email: wshou@iupui.edu

patients are found in genes encoding desmosomal proteins. Moreover, patients with desmosome mutations have a worse prognosis (7). Desmosomes, which are specialized cell–cell junction structures, help to maintain tissue integrity under high mechanical forces and thus are abundant in cardiac muscle, epithelial tissues, etc. The main components of desmosomes come from three superfamilies: desmosomal Cadherins (Desmogleins and Desmocollins), Armadillo proteins (Jup and Plakophilins) and Plakins (Desmoplakin and plectin) (8). Desmosomes are formed by the association of these three protein families: desmosomal Cadherin is linked via its cytoplasmic tail to Jup, which binds to Desmoplakin, which in turn tethers intermediate filaments to the cell membrane. Recent cardiac-specific mutation mouse models of Desmoplakin and Desmoglein 2 have recapitulated the aspects of ARVC (9–11), supporting the crucial role of the desmosome in the pathogenesis of ARVC. A homozygous 2 bp deletion of the Jup gene has been identified in Naxos patients (12). Interestingly, heterozygous *Jup*-deficient mice were reported to develop ARVC-like phenotype by aging and training (13). However, it remains elusive how this homozygous loss-of-function mutation results in ARVC.

In the current study, we have generated and characterized a cardiomyocyte-restricted *Jup* knockout mouse, which largely mimics clinical aspects of ARVC. We demonstrate that ventricular arrhythmias in this ARVC model are associated with progressive cardiomyopathy and compensatory fibrosis in *Jup*-related ARVC and that massive cell death plays a crucial role in the initiation of ARVC. We have also revealed that the elevated transforming growth factor-beta (TGFβ) signaling is associated with the pathogenesis of *Jup*-related ARVC, but Wnt/β-catenin-mediated signaling is not.

RESULTS

Generation of cardiomyocyte-restricted *Jup* mutant mice

Jup was specifically deleted in cardiomyocytes by using *Cre/loxP* technology. The targeting vector was constructed by introducing two *loxP* sites flanking exons 3–5 of the mouse *Jup* gene (Fig. 1A). The neomycin cassette was selectively removed by breeding to *EIIa-Cre* mice for generating straight floxed *Jup* mice. Southern blot confirmed the expected homologous recombination and germline transmission of the *Jup* floxed allele (Fig. 1B). The floxed mice were genotyped by polymerase chain reaction (PCR) by using the primers flanking the region of the distal *loxP* site, which is downstream of exon 5. The PCR products for the wild-type (WT) allele and the floxed allele are 221 and 255 bp, respectively (Fig. 1C). We used an *αMHC-Cre* transgenic line to ablate *Jup* in cardiomyocytes in the perinatal period before myocytes become fully differentiated (14,15). To achieve that, $Jup^{f/f}$ mice were intercrossed with $Jup^{f/+}$/*αMHC-Cre* mice to generate cardiac restrictive *Jup* knockout mice ($Jup^{f/f}$/*αMHC-Cre*). Immunofluorescence staining demonstrated the specific loss of Jup expression in $Jup^{f/f}$/*αMHC-Cre* cardiomyocytes (Fig. 1D), which was further confirmed by western blot analysis (Fig. 1E).

Cardiomyocyte-restricted ablation of *Jup* results in cardiomyopathy

The inter-cross of $Jup^{f/f}$ and $Jup^{f/+}$/*αMHC-Cre* was expected to give rise to 25% $Jup^{f/f}$/*αMHC-Cre* (designated as *Jup* mutant) offspring. Note that we designate mice with genotypes of $Jup^{f/f}$ and $Jup^{f/+}$/*αMHC-Cre* as control (Ctl) in this study, as we did not observe cardiac abnormalities in any of these mice. For most experiments, the combination of $Jup^{f/f}$ and $Jup^{f/+}$/*αMHC-Cre* mice was used as controls; the genotypes of control mice with other genotypes were listed otherwise. Genotyping of 1-week-old pups revealed that ∼22% of pups were *Jup* mutant, which is not statistically different from the expected Mendelian percentage (Supplementary Material, Table S1), indicating the absence of embryonic or neonatal lethality. Indeed, newborn *Jup* mutant hearts appeared to be histologically normal (Supplementary Material, Fig. S1). *Jup* mutants died of sudden death starting at 1 month of age, with an average life-span of 4.6 months (Supplementary Material, Fig. S2). Morphological and histological analyses indicated that *Jup* mutant hearts (2-month-old) were overtly enlarged and dilated with regional dysplasia of ventricular walls and ventricular aneurysms (Fig. 2A), which are common and characteristic features of ARVC patients (16). *Jup* mutant cardiomyocytes were markedly hypertrophic as evidenced by the increase of cardiomyocyte cross-sectional area and heart weight–body weight ratio (Fig. 2B). Remarkable enlargement of the right atrium (RA) and dilation of the RV (Fig. 2A), together with severe liver congestion (Fig. 2C), suggested the failure of right ventricular function in *Jup* mutants. The LV function of *Jup* mutant animals was also compromised as shown by echocardiographic analyses (Fig. 2D; Supplementary Material, Table S2). Cardiac fibrosis was noticeable in *Jup* mutant atria and ventricles by a bright appearance on the surface of the hearts (Fig. 2A). Trichrome staining further revealed severe fibrosis in *Jup* mutant hearts (Fig. 2E). However, a portion of *Jup* mutant mice (∼30%) exhibited moderate fibrosis by 2 months. One of the other commonly seen clinical features in ARVC patients is adipose deposition (1,9), although a number of ARVC patients with Jup mutations do not display fat deposition (17). In *Jup* mutant hearts, there was no evidence of any fat deposition in either the interstitial myocardial area or in fibrotic patches (Fig. 2F).

Given the progressive nature of ARVC, the development of cardiomyopathy in *Jup* mutant mice was further evaluated at earlier stages. At postnatal day 12, *Jup* mutant hearts appeared to be histologically normal (Fig. 3A). By postnatal day 18, cardiomyocyte dropout and fibrosis were noticeable in *Jup* mutant RVs (Fig. 3B). By 1 month, heart enlargement, extensive cardiomyocyte dropout and fibrosis were evident in *Jup* mutants (Fig. 3C). These data indicate a rapid and progressive development of cardiomyopathy in *Jup* mutants.

Cardiac arrhythmia and slow conductivity in *Jup* mutant mice

Given the cardiomyopathy and sudden death observed in *Jup* mutant mice, we speculated that normal electrophysiologic activities were disturbed in *Jup* mutant hearts. Interestingly,

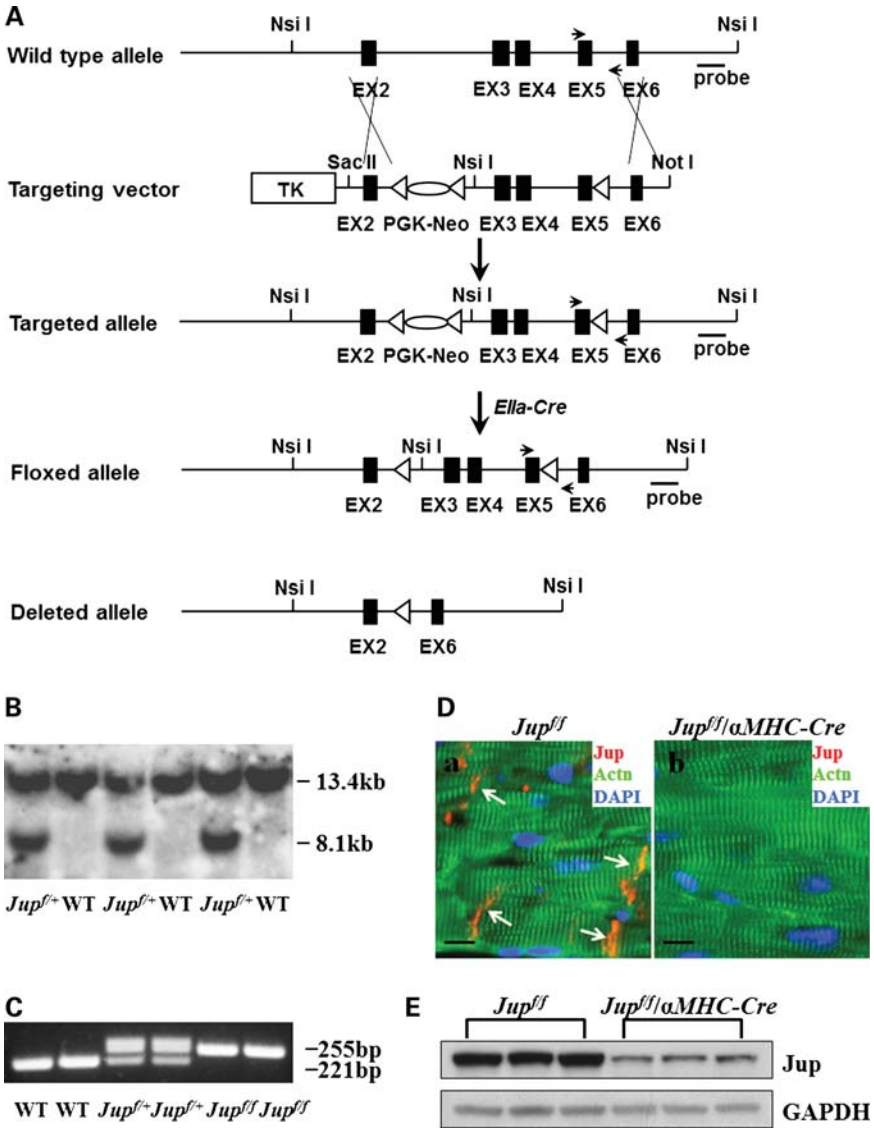

Figure 1. Generation of cardiomyocyte-restricted *Jup* mutant mice. (**A**) Schematic representation of wild type (WT), targeted and deleted alleles. *LoxP* sites are represented by triangles. Arrows denote PCR primer sites for genotyping. Probe, Southern probe site. (**B**) Southern blot analysis of WT and $Jup^{f/+}$ mice. *Nsi*I restrictive enzyme was used for digestion. The Southern probe detects a smaller (8.1 kb) band from the floxed allele in contrast to the bigger band (13.4 kb) from wild-type allele, since an extra *Nsi*I site was inserted in intron 2 of the floxed allele. (**C**) Genotypes of WT, $Jup^{f/+}$ and $Jup^{f/f}$ mice by PCR. (**D**) Immunofluorescence staining shows a specific loss of Jup signal in $Jup^{f/f}$/α*MHC-Cre* cardiomyocytes (18 days old) compared with the localization of Jup at the ICDs in littermate $Jup^{f/f}$ cardiomyocytes. Actn, α-actinin. Bars, 10 μm. (**E**) Western blot analyses of Jup protein in $Jup^{f/f}$ and $Jup^{f/f}$/α*MHC-Cre* hearts (18 days old). Glyceraldehyde 3-phosphate dehydrogenase (GAPDH) served as a total protein loading control. Densitometric analyses revealed ~70% reduction of Jup signal in $Jup^{f/f}$/α*MHC-Cre* hearts.

at postnatal day 12 when no apparent histological alteration was found, electrocardiogram (ECG) recordings were normal in *Jup* mutant hearts (Fig. 4A; Supplementary Material, Table S3). By postnatal day 18 when cardiomyocyte dropout/fibrosis was mainly noticeable in *Jup* mutant RVs, ECG revealed a decreased QRS complex amplitude in *Jup* mutant hearts (Fig. 4B; Supplementary Material, Table S4). At 1 month of age when cardiomyopathy and fibrosis developed in both ventricles, complex electrophysiological abnormalities were detected in *Jup* mutant hearts: low amplitude of the QRS complex, prolonged PR interval and spontaneous non-sustained ventricular tachycardia (VT; Fig. 4C; Supplementary Material, Table S5). By 2 months of age, in *Jup* mutants, the amplitude of the P-wave was significantly higher, the amplitude of the QRS complex was significantly lower, the PR interval was prolonged and frequent spontaneous ventricular ectopic beats (VEB) were observed (Fig. 4D; Supplementary Material, Table S6). All these electrophysiological activities in *Jup* mutant hearts were quite consistent with the corresponding histological findings at various stages (Figs 2 and 3), suggesting that the abnormal electrophysiologic activities develop along with the histopathological progression. A prolonged PR interval often suggests atrioventricular conduction abnormalities. The measurement of the conduction velocity (CV) in Langendorff-perfused hearts revealed that both CV_{max} and CV_{min} were

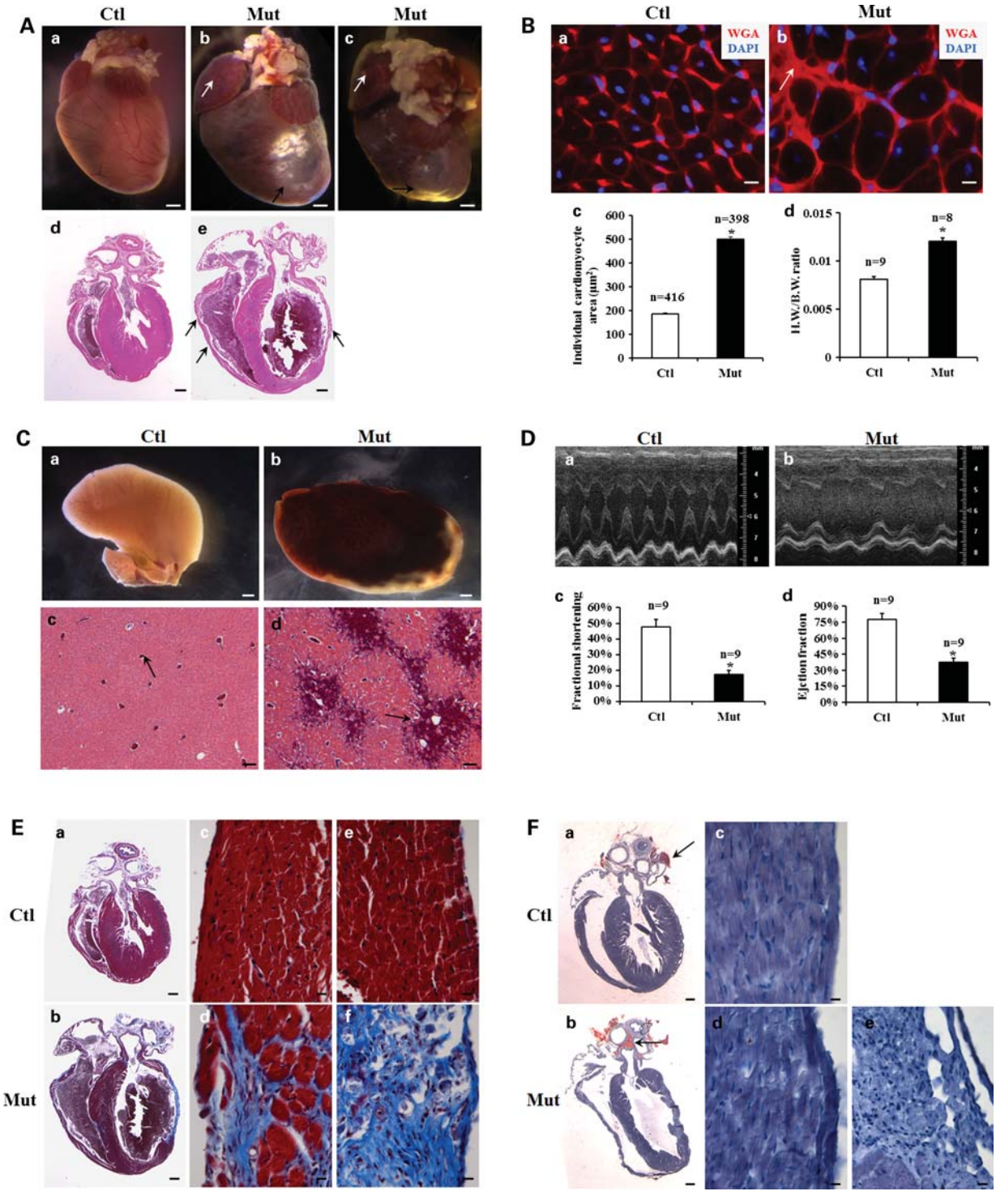

Figure 2. Cardiomyopathy and cardiac fibrosis in 2-month-old *Jup* mutant mice. (**A**) Macroscopic and microscopic phenotypes of *Jup* mutant hearts. *Jup* mutant hearts (b) and (c) show marked enlargement of right atria (white arrow) and ventricles, accompanied by ventricular aneurysms (black arrow) and massive fibrosis (bright appearance) on heart surface. Histological sections reveal dilation of RA, LV and RV in *Jup* mutant heart (e), and dysplasia of ventricular walls (black arrows). Ctl, control; Mut, mutant. Bars (a–c), 1 mm; bars (d and e), 0.5 mm. (**B**) WGA staining of cross heart sections revealed hypertrophic *Jup* mutant cardiomyocytes (b). The white arrow points to the scar area. (c) The average individual myocyte cross area of *Jup* mutant cardiomyocytes is significantly larger than that of control cardiomyocytes, $^{*}P < 0.001$; (d) heart weight/body weight (H.W./B.W.) ratio of *Jup* mutant mice is significantly higher than that of control mice, $^{*}P < 0.001$. Bars (a and b), 10 μm. (**C**) Liver congestion of *Jup* mutant mice (b) and portal vein (black arrows) dilation (d). Bars (a and b), 1 mm; bars (c and d), 0.1 mm. (**D**) Representative echocardiography shows compromised systolic function of the LV of a *Jup* mutant (b). (c) and (d) Echocardiographic analyses of fractional shortening and ejection fraction, respectively, $^{*}P < 0.001$. (**E**) Masson's trichrome staining demonstrates massive cardiac fibrosis (blue staining) in a *Jup* mutant heart in both right ventricular wall (d) and left ventricular wall (f). Bars (a and b), 0.5 mm; bars (c–f), 10 μm. (**F**) Oil Red O staining did not identify adipose deposition or infiltration in *Jup* mutant or control myocardium. Physiological fat staining is seen in aorta-surrounding fat tissue (black arrows). Bars (a and b), 0.5 mm; bars (c–f), 10 μm.

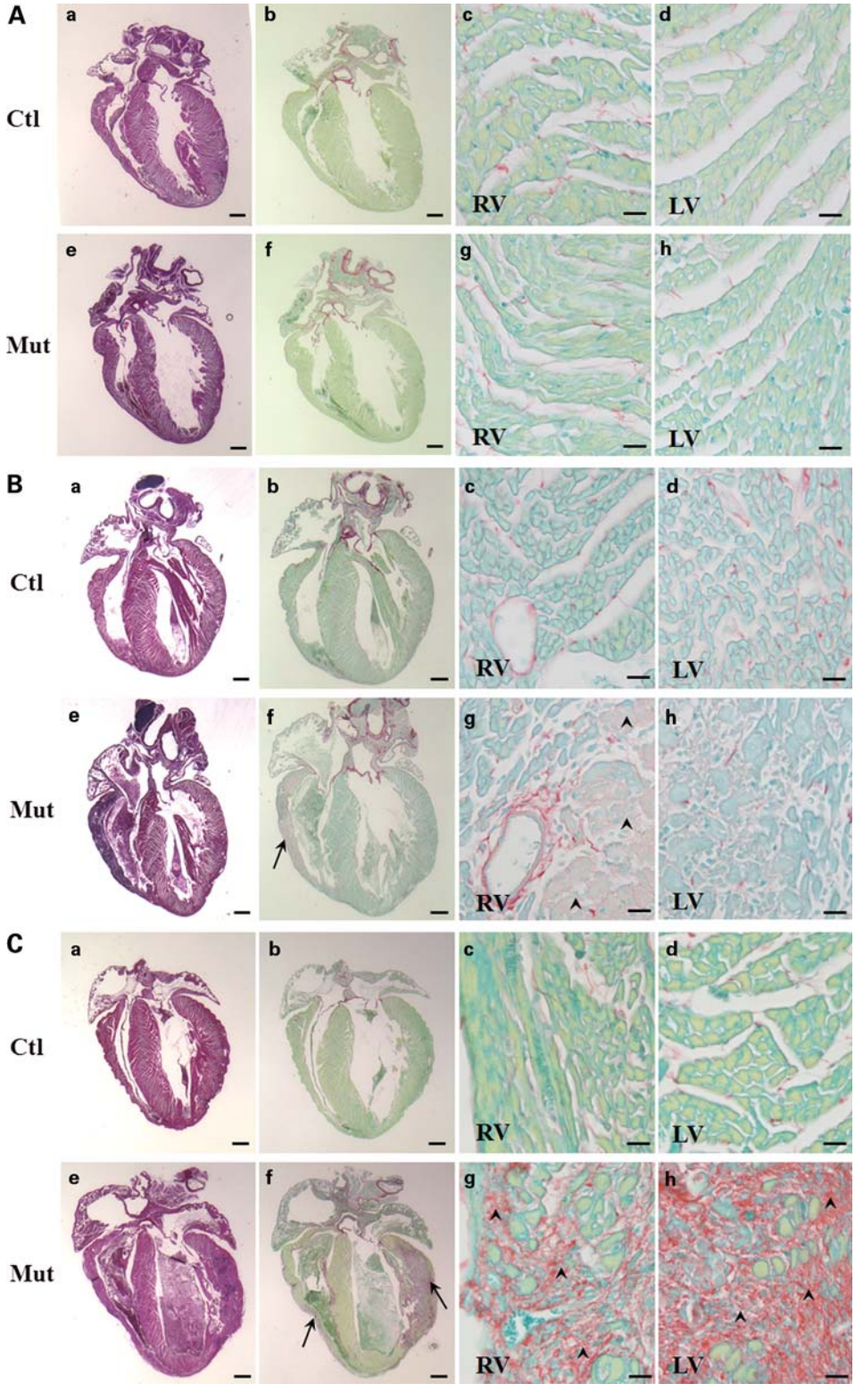

Figure 3. Progressive cardiomyopathy and fibrosis in *Jup* mutant mice. (**A**) H&E staining (a and e) and Sirius red-fast green staining (b–d and f–h) of 12-day-old hearts. (c, g) and (d, h) High magnification of RV and LV from (b) and (f), respectively. Bars (a, b, e, f), 0.5 mm; bars (c, d, g, h), 20 μm. (**B**) H&E staining (a and e) and Sirius red-fast green staining (b–d and f–h) of 18-day-old hearts. Fibrotic substitution [arrow in (f); arrowheads in (g)] is evident in *Jup* mutant RV. Bars (a, b, e, f), 0.5 mm; bars (c, d, g, h), 20 μm. (**C**) H&E staining (a and e) and Sirius red-fast green staining (b–d and f–h) of 30-day-old hearts. RA, RV and LV of a *Jup* mutant heart (e) was overtly enlarged compared to those of a littermate control heart (a). Sirius red-fast green staining demonstrates broad fibrosis (arrows in (f); arrowheads in (g, h)) in both RV (g) and LV (h). Bars (a, b, e, f), 0.6 mm; Bars (c, d, g, h), 30 μm.

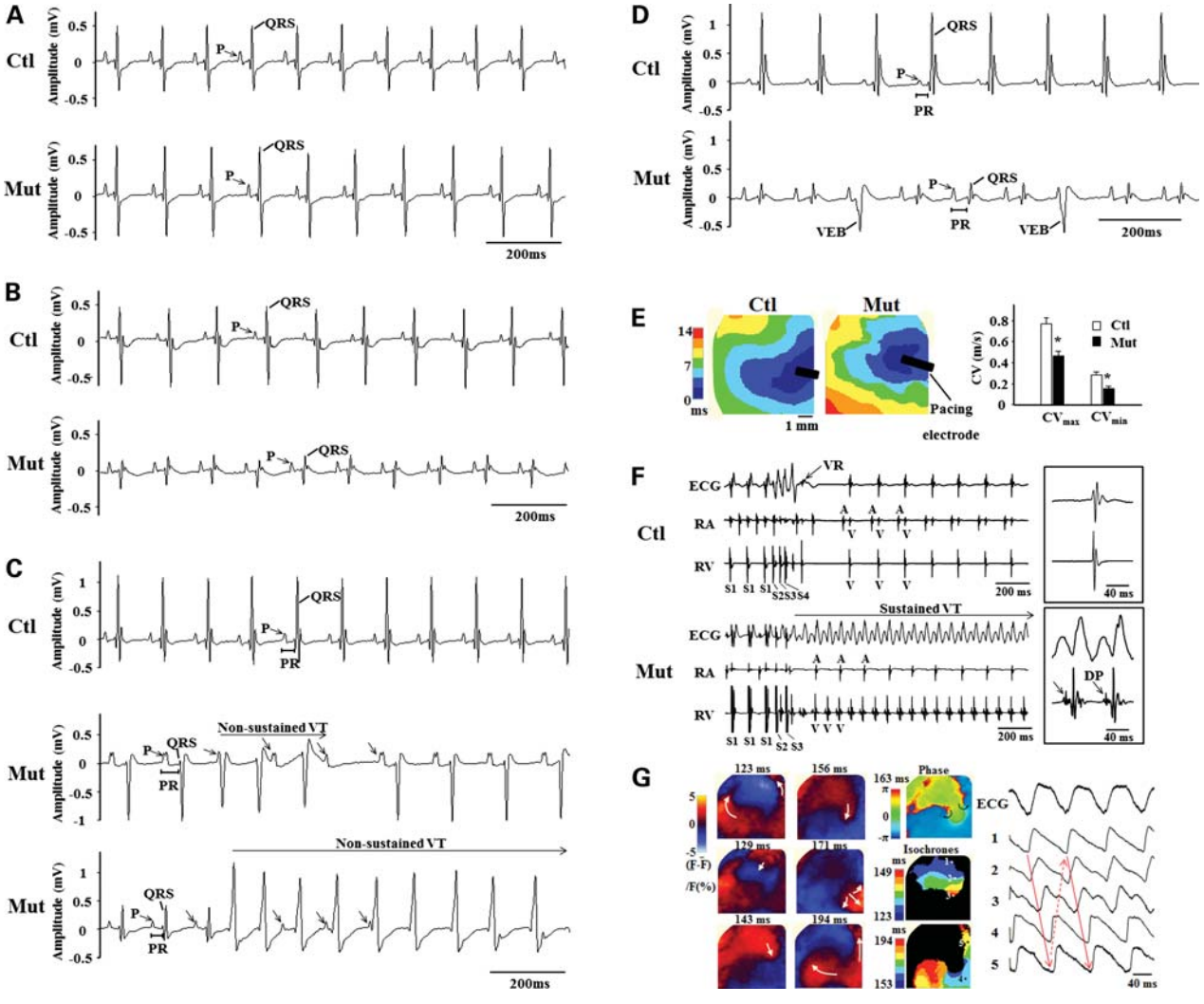

Figure 4. Cardiac arrhythmia and reduced CV in *Jup* mutant mice. (**A**) Representative surface ECG recordings of 12-day-old control and *Jup* mutant mice. (**B**) ECG recordings of 18-day-old mice. (**C**) ECG recordings of 30-day-old mice. A horizontal bar in the middle tracing marks a 3-beat run of spontaneous non-sustained VT in a *Jup* mutant. Arrows point to dissociated P-waves. VT in the other *Jup* mutant (bottom) lasted for 2 s before spontaneously converting to normal sinus rhythm. (**D**), ECG recordings of 2-month-old mice. VEBs are evident in *Jup* mutants exhibiting wide QRS complexes that occur without apparent association with P-waves. (**E**) Representative isochrones of ventricular activation during RV epicardial pacing in *Jup* mutant and control hearts are shown on the left panel. The maximal CV (CV_{max}) and minimal CV (CV_{min}) are shown on the right panel. Data are presented as Mean $\pm$ SEM. $^{*}P < 0.005$. (**F**) A global ECG, intracardiac electrograms of the RA and RV during ventricular extra-stimuli in 5-month-old *Jup* mutant and control hearts. Note that sustained VT was induced in *Jup* mutant hearts by two extra-stimuli (S1 cycle length: 100 ms; S1–S2: 60 ms; S2–S3: 60 ms), while only a single ventricular response was seen in control hearts even with a more aggressive pacing protocol (S1 cycle length: 100 ms; S1–S2: 50 ms; S2–S3: 40 ms, S3–S4: 30 ms). Expanded tracings of ECG and intra-RV electrogram during the VT (right bottom panel) show fragmented DPs in the RV local bipolar electrogram. An expanded tracing of normal ECG in controls is shown in right upper panel. (**G**) Membrane voltage (V_m) optical signals from the RV epicardial surface during the sustained VT in a *Jup* mutant heart. Left panels show snapshots of V_m ratio maps where depolarization and repolarization are shown in red and blue, respectively. Numbers indicated above each map denote times from the start of data acquisition. Note: there is a figure-of-eight reentry during the VT. Middle panels show a phase map (top) and isochrones for the central common pathway (middle) and outer reentrant circuits (bottom) of the VT. Two phase singularities were present at both ends of the central common pathway (black circle arrows in the phase map). Right panels show ECG and local V_m optical signals obtained at sites indicated in the isochronal maps during the VT.

significantly reduced in *Jup* mutants (Fig. 4E). Besides spontaneous VT, another characteristic of ARVC is the inducibility of VT, which is also the leading cause of sudden death in ARVC patients (18). Sustained monomorphic VTs (VT cycle length: 69 $\pm$ 4 ms, VT duration: 61 $\pm$ 16 s) were reproducibly induced by bust or programmed ventricular stimulation in six of the seven *Jup* mutant hearts, but in none of the five control hearts (Fig. 4F). In two *Jup* mutant hearts, sustained VTs with different QRS morphologies were induced separately. Fragmented diastolic potentials (DPs) were noted in RV intracardiac bipolar electrograms during the VT in two *Jup* mutant hearts (Fig. 4F). In one *Jup* mutant heart, a figure-of-eight reentry in the epicardial RV surface was observed during the sustained VT (Fig. 4G).

Loss of desmosomes in *Jup* mutant hearts

There are three types of specialized cell–cell junctional structures localized to the intercalated discs (ICDs): desmosomes, adherens junctions and gap junctions. Jup is a

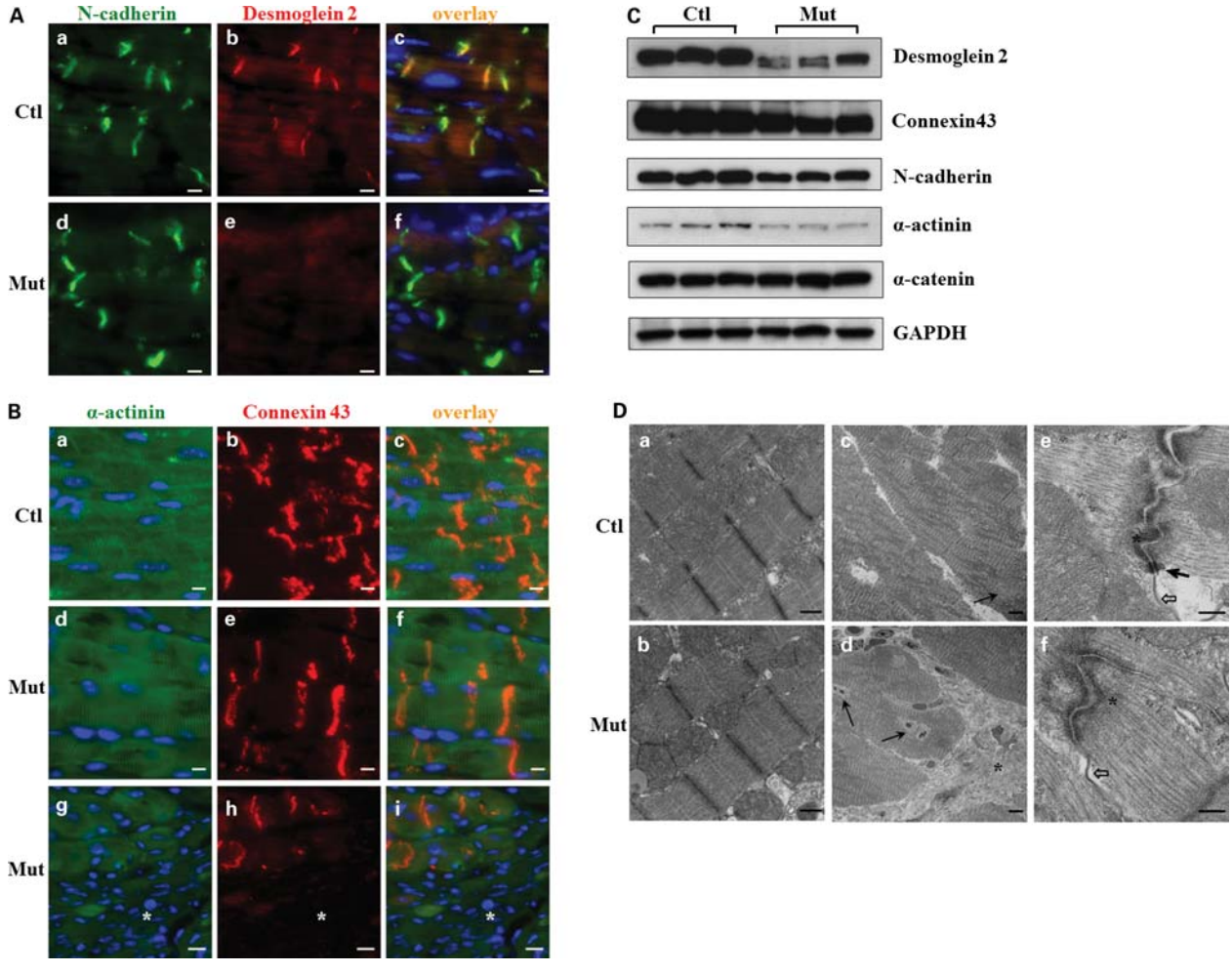

Figure 5. Analyses of cell–cell junctions in 2-month-old *Jup* mutant mice. (**A**) Desmoglein 2 staining signal was lost at the *Jup* mutant intercalated discs (ICDs), whereas N-cadherin staining was similar between *Jup* mutant and control hearts. Bar, 10 μm. (**B**) Connexin 43 staining was normal in *Jup* mutant cardiomyocytes, but lost in the scar area (asterisk). Bars, 10 μm. (**C**) Western blot analyses of cell junction proteins. (**D**) TEM analyses reveal normal sarcomere structure in *Jup* mutant cardiomyocytes (b). Replacement of cardiomyocytes by collagen deposition (asterisk) in *Jup* mutant hearts (d). Black arrows point to the cardiomyocyte nuclei. (e) and (f) Normal adherens junction (asterisk) and gap junction (white arrows) at *Jup* mutant ICDs, whereas no desmosomes are identified in *Jup* mutant hearts, as opposed to typical desmosomes (black arrow) in control hearts. Bars (a and b), 500 nm; bars (c and d): 5 μm; bars (e and f): 250 nm.

component for both desmosomes and adherens junctions. Immunofluorescence staining of several specific junctional components was performed in 2-month-old heart sections. The staining of N-cadherin, a component for adherens junctions, exhibited a similar pattern in *Jup* mutant hearts and control hearts (Fig. 5A). In contrast, the staining signal of Desmoglein 2, a Cadherin homolog in desmosomes and a Jup binding protein, was lost in *Jup* mutant ICDs (Fig. 5A), indicating a potential disruption of desmosome structure. Staining of Connexin 43, a central protein component for gap junctions, was unaffected in the ICDs of *Jup* mutant cardiomyocytes (Fig. 5B). Expectedly, the expression of Connexin 43 was lost in the scar area where extensive cardiomyocyte dropout occurred (Fig. 5B). The western blot analyses revealed that Desmoglein 2 was greatly reduced in its abundance and was also downshifted in protein size (Fig. 5C), suggesting that Desmoglein 2 is unstable and degraded when it loses its binding to Jup. The decrease in total levels of Connexin 43 and N-cadherin in *Jup* mutant hearts was consistent with the significant cardiomyocyte loss (Fig. 5B), which was also evident by the reduction of total α-actinin, a specific sarcomeric-binding protein for cardiomyocytes. As an internal control, there was no noticeable difference in the total levels of α-catenin, a central cell–cell junctional protein for all types of cells which form adherens junctions, e.g. cardiomyocytes, endothelial cells, fibroblasts etc. To directly address the impact of Jup on cell–cell junctions, transmission electron microscopy (TEM) analyses were performed in 2-month-old hearts. *Jup* mutant sarcomeres appeared to be normal (Fig. 5D). However, a significant number of mutant cardiomyocytes were surrounded by collagen deposits consistent with the histological findings (Figs 2 and 3). Adherens junctions and gap junctions appeared to be normal in *Jup* mutant hearts (Fig. 5D). In contrast, no typical desmosomes were identified after screening

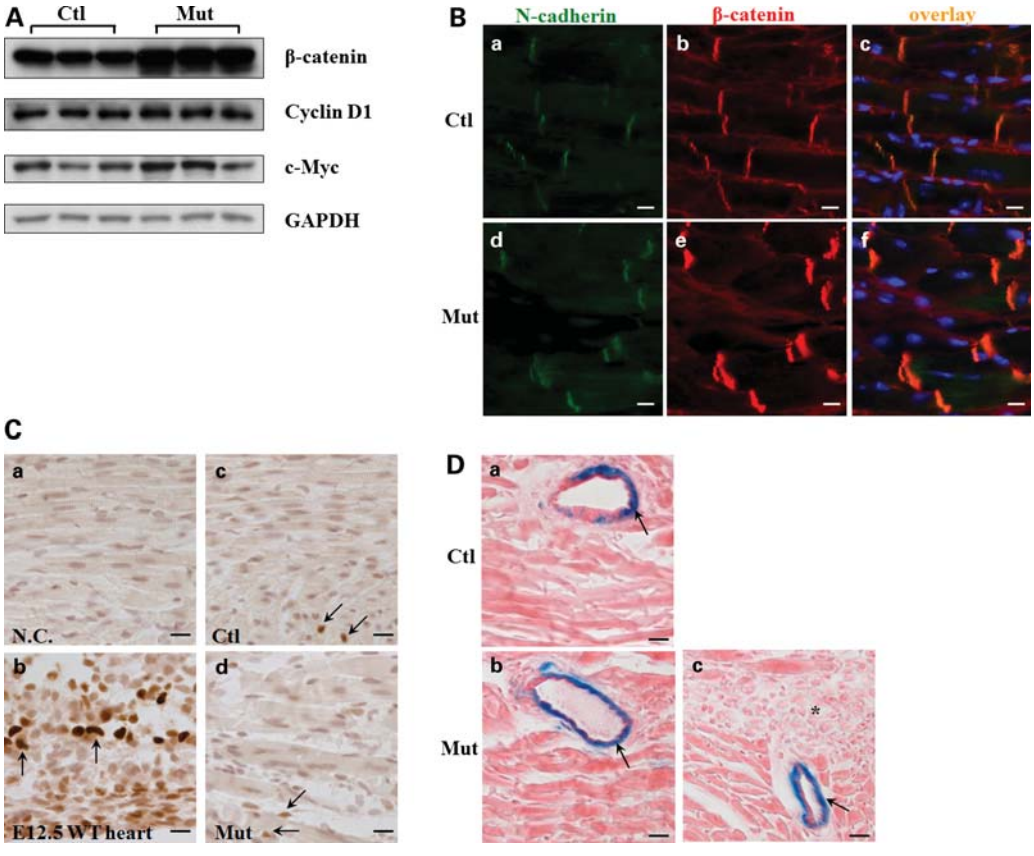

Figure 6. Increased β-catenin at cell adhesion without affecting Wnt/β-catenin signaling in *Jup* mutant mice. (**A**) Western blot of total β-catenin and its signaling targets—Cyclin D1 and c-Myc. (**B**) Immunofluorescence staining of β-catenin in 18-day-old *Jup* mutant and control hearts. Note marked increase in expression of β-catenin in *Jup* mutant ICDs compared with that in control ICDs, no signal was detectable in nuclei or cytosols in either *Jup* mutant or control cardiomyocytes. Bars, 10 μm. (**C**) Immunostaining of Cyclin D1 in *Jup* mutant and control hearts (18 days old). (a) Serves as a negative control (without primary antibody incubation). (b) Positive Cyclin D1 staining (dark brown staining in nuclei indicated by arrows) is shown in embryonic day 12.5 (E12.5) WT cardiomyocytes. Positive stainings (arrows) are identified in some non-cardiomyocytes in both control (c) and *Jup* mutant (d) hearts. These non-cardiomyocytes are different from cardiomyocytes by presenting non-rod shape nuclei and localizing at the muscle bundle periphery. Note that no positive stainings were detectable in either control or *Jup* mutant cardiomyocytes. Bars, 20 μm. (**D**) Representative pictures of X-Gal staining of a 18-day-old $Jup^{f/f}$/*Fos-LacZ* heart (a) and a 18-day-old $Jup^{f/f}$/*αMHC-Cre/Fos-LacZ* heart (b and c). There is no signal in cardiomyocytes in either control or *Jup* mutant cardiomyocytes, nor is in scar tissues (asterisk) (c). In contrast, X-Gal staining signals (arrows) are apparent in vascular cells. Bars, 20 μm.

numerous sections (Fig. 5D), in agreement with the loss of Desmoglein 2 localization to *Jup* mutant ICDs (Fig. 5A).

Increase of β-catenin at ICDs without affecting Wnt/β-catenin signaling in *Jup* mutant hearts

β-Catenin is a close homolog of Jup, both have multiple central armadillo repeats and are capable of forming cell adhesion complexes (adherens junctions) and mediating Wnt signaling (19). It is also well known that Jup but not β-catenin is a structural component of desmosomes in normal physiological conditions (19,20). Furthermore, it has been suggested that disrupted Wnt/ β-catenin signaling plays a causal role in the pathogenesis of ARVC (9). Therefore, it is of interest to know whether/how β-catenin and its mediated signaling is affected by the loss of Jup. Interestingly, we found that β-catenin was up-regulated in *Jup* mutant hearts (Fig. 6A). Immunostaining revealed that β-catenin was present exclusively at the ICDs in both control and *Jup* mutant hearts, but not in the cytosol or nucleus (Fig. 6B). The staining intensity of β-catenin in *Jup* mutant ICDs was much stronger than that in control ICDs (Fig. 6B), consistent with the finding by western blot analysis (Fig. 6A). The lack of nuclear β-catenin suggested that β-catenin signaling was not significantly altered in *Jup* mutant hearts. To further confirm this finding, we analyzed the expression levels of two known β-catenin down-stream targets, Cyclin D1 and c-Myc, and found similar levels between *Jup* mutant and control hearts (Fig. 6A). Additionally, Cyclin D1 staining in cardiomyocytes did not display any noticeable difference between *Jup* mutant and control hearts (Fig. 6C), apart from the observation that positive staining signals were very rare in these postnatal cardiomyocytes, which was consistent with a previous report (21). Since Cyclin D1 and c-Myc are regulated by many other signal transduction pathways, a specific β-catenin signaling reporter mouse line—*Fos-LacZ* transgenic mouse (22)—was used to examine β-catenin transcriptional activities *in vivo*. The X-Gal staining was similar in *Jup* mutant and control hearts with no detectable signal in cardiomyocytes, in contrast to the distinct positive staining in vascular cells

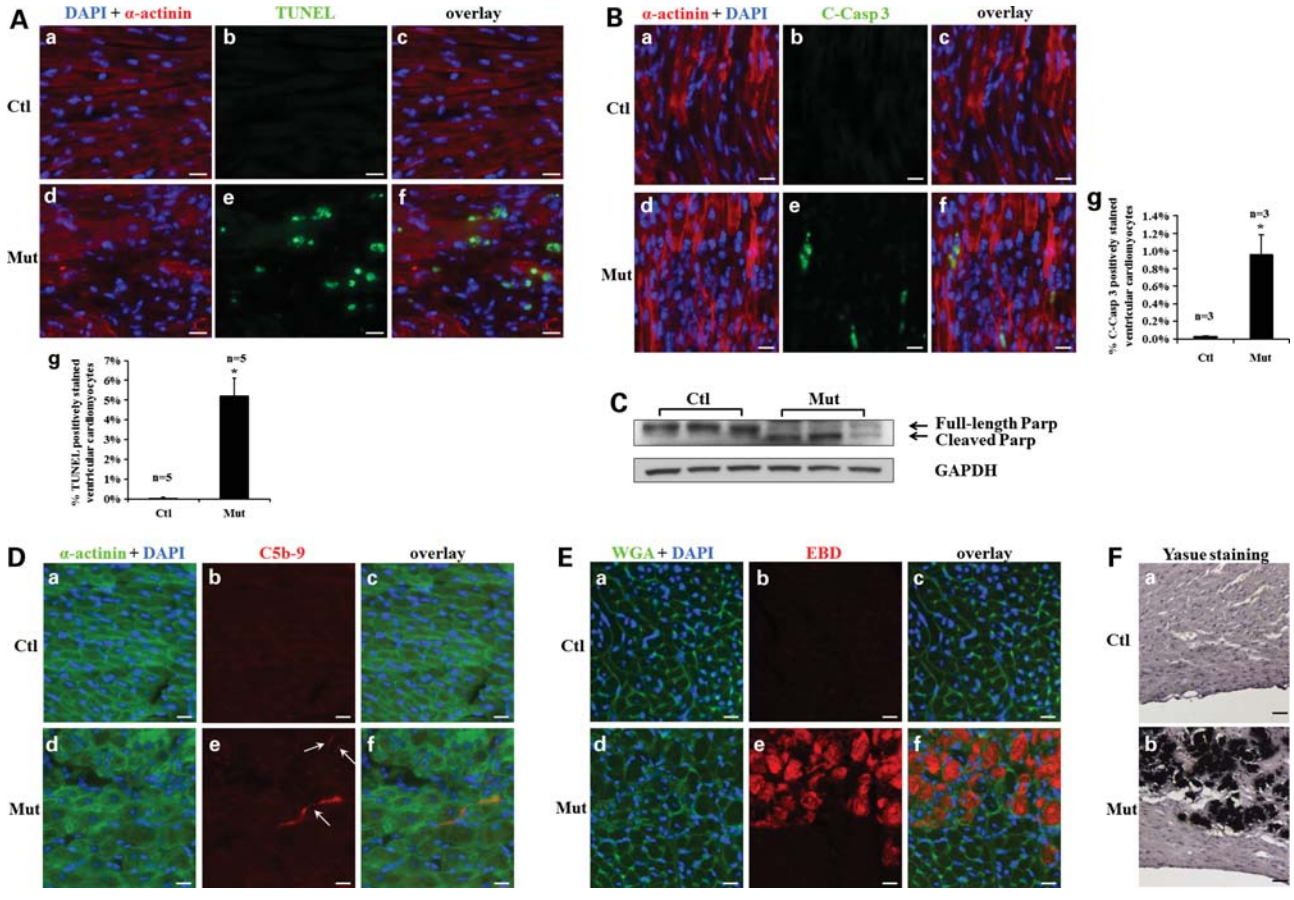

Figure 7. Cell death of *Jup* mutant cardiomyocytes. (**A**) Massive cell death in 18-day-old *Jup* mutant hearts detected by TUNEL staining. The quantitative data are shown in (g). $^{*}P < 0.001$, compared with controls. Bars, 20 μm. (**B**) Enhanced apoptosis in *Jup* mutant hearts detected by cleaved Caspase 3 (C-Casp 3) staining. Quantitation is shown in (g), $^{*}P < 0.05$, compared with controls. Bars, 20 μm. (**C**) Cleaved PARP was seen in *Jup* mutant hearts. (**D**) C5b-9 signals were evident on the sarcolemma of 18-day-old *Jup* mutant cardiomyocytes. Arrows in (e) denote the positive C5b-9 signals in *Jup* mutant cardiomyocytes. Bars, 20 μm. (**E**) Histochemical analyses of 19-day-old mice injected with EBD. Note the area with EBD-positive signals in *Jup* mutant hearts was also severely disorganized. Bars, 20 μm. (**F**) Calcification of 2-month-old *Jup* mutant ventricular myocardium. Calcification was shown as black signal by Yasue staining. Nuclei were counterstained with Hematoxylin. Bars, 20 μm.

(Fig. 6D). There was no obvious positive X-Gal staining signal in fibrotic areas in *Jup* mutant hearts. (Fig. 6D). Collectively, these data suggest that the enhanced expression of β-catenin in *Jup* mutant hearts primarily compensates for the loss of Jup in the constitution of adherens junction in the ICDs without altering overall β-catenin transcriptional activities in *Jup* mutant cardiomyocytes.

Increased cardiomyocyte death in *Jup* mutant hearts

We speculated that massive cardiomyocyte dropout in *Jup* mutant hearts resulted from cell death, which was likely triggered by the cell–cell dissociation following desmosome disruption. Indeed, we found extensive cardiomyocyte death in 18-day-old *Jup* mutant hearts evidenced by the TdT-mediated dUTP nick end labeling (TUNEL) assay (Fig. 7A). We noted that cell death was usually confined to the areas proximal to fibrotic replacement areas. Since the TUNEL assay can detect both cell necrosis and apoptosis (23), next we determined whether *Jup* mutant cardiomyocytes underwent apoptosis or necrosis or both. Cleaved (active) Caspase-3 staining demonstrated enhanced apoptosis in *Jup* mutant cardiomyocytes (Fig. 7B), which was further confirmed by the accumulation of cleaved poly ADP ribose polymerase (PARP), a substrate of active Caspase-3, in *Jup* mutant hearts (Fig. 7C). One of the hallmarks of cell necrosis is the loss of membrane integrity, which does not occur in cell apoptosis. Deposition of C5b-9 (a component of complement membrane attack complex) on cell membrane leads to cell membrane lysis, and thus the membranous localization of C5b-9 is used as a specific indication for myocardial necrosis (24). A typical way to test the sarcolemmal integrity *in vivo* is to inject mice with Evans Blue Dye (EBD), a large tracking molecule that can only enter into myocyte cytoplasm when the sarcolemma is disrupted (25). Indeed, regional myocyte necrosis was evident in *Jup* mutant hearts as shown by positive signals of C5b-9 and EBD in *Jup* mutant ventricular myocytes (Fig. 7D and E). Myocardial calcification, an obligate consequence of cell necrosis, was also apparent in 2-month-old *Jup* mutant ventricles (Fig. 7F). Following the massive cell death, inflammatory cells (e.g. neutrophils and macrophages) were observed to have infiltrated into the *Jup* mutant

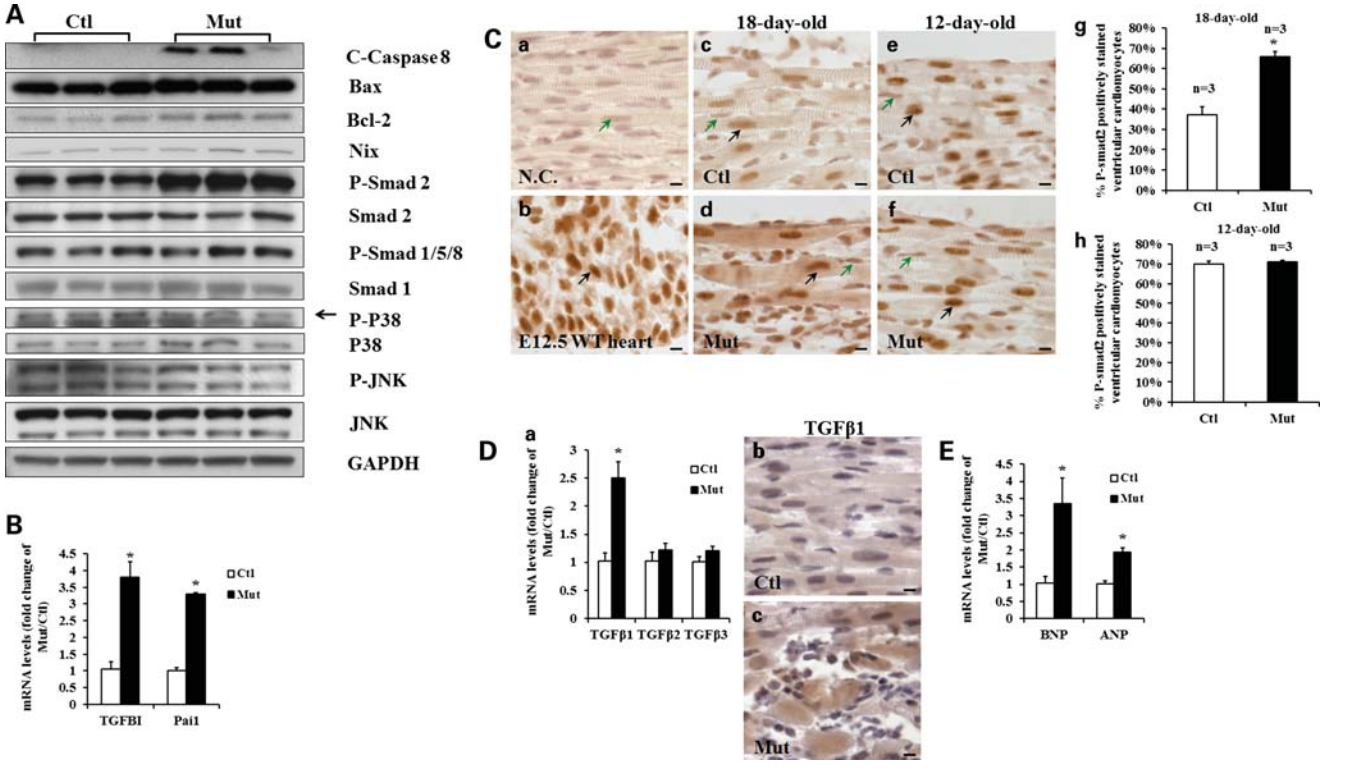

Figure 8. Alteration of TGFβ signaling in *Jup* mutant hearts. (**A**) Western blotting analyses of potential alteration of signaling in regulating cell death in 18-day-old *Jup* mutant hearts. (**B**) qRT-PCR analyses of TGFBI and Pai1 in 18-day-old *Jup* mutant hearts ($n = 3$) and control hearts ($n = 3$). $P < 0.05$, compared with controls. (**C**) P-Smad2 signal in *Jup* mutant cardiomyocytes. A negative control (NC, without first antibody) and a positive control (an E12.5 embryonic heart) are shown in (a) and (b), respectively. Black arrows denote positively stained cardiomyocytes and green arrows denote negatively stained cardiomyocytes. At the age of 18 days old, *Jup* mutant cardiomyocytes (d) displayed much stronger P-Smad2 signals than littermate controls (c). The percentage of positively stained cardiomyocytes was also significantly higher in *Jup* mutant hearts than control hearts (g), $^*P < 0.01$, compared with controls. In contrast, at the age of 12 days, both *Jup* mutant (f) and control (e) cardiomyocytes displayed similar P-Smad2 staining signals. The percentage of positively stained ventricular cardiomyocytes is quantified in (h). Bars, 10 μm. (**D**) Increased TGFβ1 expression in 18-day-old *Jup* mutant hearts. (a) qRT-PCR analyses revealed that mRNA levels of TGFβ1, but not TGFβ2 or TGFβ3, were significantly increased in *Jup* mutant hearts ($n = 3$) compared with controls ($n = 3$). $^*P < 0.05$. The TGFβ1 immunoreactive signal is evident in the cytoplasm of *Jup* mutant cardiomyocytes (c), in contrast to the weak/background signal in control cardiomyocytes (b). Bars, 10 μm. (**E**) Elevation of BNP and ANP in 18-day-old *Jup* mutant hearts ($n = 3$), compared with control hearts ($n = 3$) analyzed by aRT-PCR. $^*P < 0.05$.

ventricular myocardia (Supplementary Material, Fig. S3). In consistent, the expression of proinflammatory cytokines IL-1β and IL-6 were significantly increased in *Jup* mutant hearts. Interestingly, no apoptosis or necrosis was detected in 12-day-old *Jup* mutant hearts (data not shown). These findings were in agreement with the histological findings (Fig. 3). As expected, we did not detect significant proliferation of cardiomyocytes in either 18-day-old *Jup* mutant or control hearts (Supplementary Material, Fig. S4).

Potential alteration of cell-death-related signaling in *Jup* mutant hearts

Next, we sought to investigate what potential signaling pathways were associated with the massive cell death observed in *Jup* mutant cardiomyocytes. First, we found that the cell death was triggered extrinsically rather than intrinsically through the mitochondrial path, since cleaved (active) Caspase 8, which is dedicated to the extrinsic pro-apoptotic pathway (26), was elevated in *Jup* mutant hearts, whereas there was no overt difference in abundance of Bax or Nix (proteins engaged in intrinsic cell apoptosis and/or necrosis) (27) between *Jup* mutant and control hearts (Fig. 8A). Next, we investigated what cell-death-related-signaling pathways were likely affected. Mitogen-activated protein kinase (MAPK) and C-Jun N-terminal kinase (JNK) have been known for their implication in cell-death-signaling transduction (28). The contribution of TGFβ signaling to cell death has also been well documented in addition to its critical role in eliciting fibrosis (29,30). We found that the activities of P38 MAPK and JNK were not different between 18-day-old *Jup* mutant and control hearts (Fig. 8A). In contrast, phospho-Smad2 (P-Smad2) was increased in *Jup* mutant hearts, whereas phospho-Smad1/5/8 (P-Smad1/5/8), which reflects BMP-mediated signaling (31), was comparable between *Jup* mutant and control hearts. The up-regulation of TGFβ signaling in *Jup* mutant hearts was further supported by the finding of enhanced expression of TGFBI (TGFβ-induced) and Pai1 (Plasminogen activator inhibitor type 1) (Fig. 8B), bona fide TGFβ-signaling downstream effector molecules (32). Phospho-Smad2 immunostaining further revealed the elevation of TGFβ signaling in *Jup* mutant cardiomyocytes (Fig. 8C). Interestingly, at postnatal day 12, when there were no discernible histological or electrophysiological

abnormalities in *Jup* mutant hearts, there was no significant difference in phospho-Smad2 signal between *Jup* mutant and control cardiomyocytes (Fig. 8C), suggesting that the altered TGFβ signaling is closely associated with the pathological process, but not with *Jup* deficiency *per se*. There are three TGFβ isoforms expressed in mammals, designated TGFβ1, TGFβ2 and TGFβ3 (33). Interestingly, we found that the expression of TGFβ1 was significantly increased in *Jup* mutant hearts, but not TGFβ2 or TGFβ3 (Fig. 8D). The immunostaining further confirmed the elevation of TGFβ1 in *Jup* mutant cardiomyocytes (Fig. 8D). It has been shown that mechanical stress agonists induce a strong TGFβ-signaling response (34). We believe that the disruption of desmosomes in *Jup* mutant myocardium generates significant mechanical stress in the myocardial wall, which triggers TGFβ signaling. Indeed, both B-type natriuretic peptide (BNP) and atrial natriuretic peptide (ANP), well-known wall stress biomarkers, were significantly increased in 18-day-old *Jup* muant hearts (Fig. 8E).

DISCUSSION

ARVC has been considered as a disease of the desmosome, since mutations in desmosome genes have been identified in a large percentage of ARVC patients (7). Several mouse models harboring mutations in other desmosome proteins have recapitulated several aspects of ARVC (9–11), strongly supporting the pathophysiological roles of desmosome disruption in ARVC patients. However, it has also been noted that different mutations in the same desmosome gene or in different desmosome genes have distinct clinical presentations, prognoses or inheritance patterns (35).

Naxos disease is associated with a homozygous 2 bp (2157T and 2158G) deletion, which causes a frame shift and premature termination of translation. The truncated Jup mutant protein (with incomplete armadillo repeats) fails to localize at the ICDs of Naxos patients (17). Our current myocardial *Jup* conditional knockout mouse model largely mimics the cardiomyopathy and arrhythmias seen in Naxos disease: cardiac dysfunction, myocyte dropout, ventricular dilation and aneurysm, cardiac fibrosis and spontaneous ventricular arrhythmias. We noticed that there was a variability in those phenotypes, which was likely attributable to the mixed 129Sv/C57 background of mice and/or the variability of Cre-mediated homologous recombination efficiency. However, adipose tissue deposition was never found in *Jup* mutant mice, which is different from typical ARVC clinical presentation, although the presence and the degree of fat deposition or infiltration in ARVC patients vary greatly (17,36). Notably, fat infiltration into normal right ventricular myocardium naturally occurs in >50% of elderly people (37). Thus, adipose replacement of the myocardium is not an obligate diagnostic criterion for ARVC (36). The absence of fat deposition in mutant myocardium may also be attributable to species difference: a normal mouse heart does not have epicardial fat, whereas there is physiological sub-epicardial fat in a normal human heart (10). Ultra-structural analyses have revealed the absence of desmosome structure in *Jup* mutant ICDs, which is similar to the ultra-structural findings of desmosome disruption in ARVC patients with desmosome gene mutations (38), supporting the pathophysiological role of desmosome disruption in ARVC.

In contrast to our findings, a recent report of cardiac-specific knockout of *Jup* using a cardiac inducible *αMHC/MerCreMer* transgenic line demonstrated much milder cardiac phenotypes in *Jup* cardiac-deficient mice: cardiomyopathy developed 5 months after the administration of tamoxifen (which was given at 6–8 weeks of age), there was no spontaneous or induced cardiac arrhythmia, and >50% *Jup* cardiac-deficient mice survived 17 months after the administration of tamoxifen (39). Ultra-structurally, desmosomes, although presented as atypical morphologies, were formed in tamoxifen-induced *Jup*-deficient hearts (39). The discrepancy may largely be attributed to the lower genetic ablation efficiency by tamoxifen induction (in comparison to the rigorous endogenous *αMHC*-Cre activity) and/or ablation of *Jup* at late stages (administration of tamoxifen at 6–8 weeks of age in contrast to the persistent *αMHC*-Cre activity during perinatal and postnatal periods). Nonetheless, it is more physiologically relevant to ablate *Jup* at early postnatal stages, given that ARVC predominantly affects the young.

Jup mutant mice showed a biventricular cardiomyopathy with an early and severe hit on the RV, which seemingly contradicts the term 'ARVC'. In fact, the LV is frequently affected in ARVC patients (40). Recent studies also identified patients with left-sided arrhythmogenic ventricular cardiomyopathy with minimal or no involvement of the RV (41,42). All these clinical observations support a broad definition of 'arrhythmogenic cardiomyopathy' (1). Ventricular arrhythmia (especially VT) has been one of the crucial, though not exclusive, characteristics of ARVC patients. It is also highly associated with sudden death in ARVC patients (18). *Jup* mutant mice developed spontaneous ventricular arrhythmia (including non-sustained VT) and slow conductivity with disease progression and also displayed VT after stimulation (Fig. 4). Interestingly, *Jup* mutant mice did not acquire ventricular arrhythmia or slow conductivity at the early stage when the heart was structurally intact, indicating that ventricular arrhythmia arose from the compromised heart integrity, as opposed to a hypothesis that arrhythmogenecity and cardiomyopathy are separate entities (43). Given the pivotal role of gap junctions in mediating electrical coupling between myocytes, it is plausible that their disruption would contribute to the arrhythmia and conduction abnormality seen in ARVC. Our data demonstrated that gap junctions and the immunoreactivity of Connexin 43 were normal in healthy *Jup* mutant myocardia. Similar findings were also observed in Desmoplakin and Desmoglein 2 mutant mice (10,11). As expected, Connexin 43 expression at the ICDs was completely lost in the myocyte dropout/fibrotic replacement region, which was consistent with our cardiac electrophysiological findings.

Besides being a structural component of desmosomes, Jup also participates in the constitution of another cell–cell junction—the adherens junction. Interestingly, Jup and β-catenin are interchangeable in adherens junctions, whereas Jup but not β-catenin is a building block for desmosomes in normal physiological conditions (19). In *Jup* mutant hearts, we found that β-catenin was significantly increased in the ICDs (Fig. 6). Ultra-structural analyses revealed the presence of intact adherens junctions in *Jup* mutant ICDs, albeit with

the absence of desmosomes. These findings suggest that the increase of β-catenin compensates for the loss of Jup in adherens junction constitutions, but not in desmosomes. Interestingly, this β-catenin compensation at adherens junctions was also observed in $Jup^{-/-}$ skin (20). Jup has also been postulated to play an inhibitory role in regulating canonical Wnt/β-catenin-signaling transduction based on its high homology with β-catenin in protein sequence and on its sharing the same protein degradation machinery with β-catenin, although the existing studies are still quite controversial (19). Recent mouse studies have suggested that the inhibition or up-regulation of Wnt/β-catenin signaling contributes to the pathogenesis of ARVC (9,39). However, we did not find any nuclear β-catenin or noticeable T-cell factor (TCF)/lymphoid enhancer factor activity in postnatal cardiomyocytes, or any difference in Wnt/β-catenin-signaling activities between *Jup* mutant and control cardiomyocytes at the early stage when myocyte death occurred. Interestingly, recent studies of postnatal cardiomyocyte-restricted ablation or stabilization of β-catenin did not demonstrate ARVC-like phenotype or any signs of massive cardiomyocyte death (44,45). Collectively, these findings do not support that Wnt/β-catenin signaling plays a pivotal causal role in the pathogenesis of *Jup*-related ARVC.

One prevailing hypothesis for the pathogenesis of ARVC is that the disruption or the absence of desmosomes renders cardiomyocytes incompetent of handling the high mechanical stresses (i.e. contracting forces and hemodynamic shearing forces), which ultimately leads to myocyte disassociation. The detached myocytes undergo cell death followed by inflammation and fibrosis. Indeed, accumulating evidence of myocyte death has been reported in ARVC patients at the early and symptomatic phases of the disease (1,46). Our *Jup* mutant mouse model recapitulated many of these pathological processes, favoring the idea that cell death triggered by desmosome disruption plays a crucial role in the pathogenesis of the disease.

TGFβ signaling is complex and imposes on many fundamental developmental, physiological and pathological processes throughout different species. It has been well documented that TGFβ signaling regulates myocyte cell death, including both apoptosis and necrosis, in addition to its paramount influences on cardiac fibrosis and hypertrophy (47,48). Interestingly, over-expression of TGFβ1 in cardiomyocytes in mice is sufficient to induce cardiomyocyte cell death and cardiac fibrosis over time (49). Moreover, the regulatory mutations in TGFβ3 have been identified in ARVC patients and the mutations render up-regulation of TGFβ3 promoter activity (6). Consistent with all these existing experimental and clinical implications of TGFβ signaling in the pathogenesis of cardiomyopathy, we found that TGFβ signaling was up-regulated in *Jup* mutant cardiomyocytes. Our data also suggest that the enhanced TGFβ activities in *Jup* mutant hearts appear to be triggered by the intensified myocardial wall stress due to the compromised cell–cell mechanical coupling upon the breakdown of the desmosome. However, given the heterogeneous genetics of ARVC, our current findings may not be transferable to other ARVCs with different genetic mutations. Further studies are needed to assess whether the enhancement of TGFβ signaling contributes to the pathogenesis of other genetic forms of ARVC. Additionally, it is of interest to investigate how the inhibition of TGFβ signaling hinders the progression of ARVC, which is currently under investigation.

In summary, *Jup* mutant mice largely recapitulate pathophysiological features of human ARVC. Our data demonstrate that myocyte death plays a key role in initiating Jup-related ARVC and that up-regulation of TGFβ signaling is likely associated with the pathogenesis of Jup-related ARVC. Our study has provided mechanistic insights which may help to improve therapeutic interventions for ARVC.

MATERIALS AND METHODS

Generation of floxed Jup mice

A *Jup* genomic clone was screened from a mouse 129SvEv genomic BAC library (RPCI-22 129 mouse library from BAC/PAC Resources, Children's Hospital Oakland) using a *Jup* probe. The targeting vector contained two *loxP* sites, which flanked the neomycin selection cassette (Fig. 1A). A fragment including part of *Jup* introns 2–6 with the third *loxP* site inserted into intron 5 was engineered downstream of the neomycin selection cassette. Linearized targeting vector (25 μg) was electroporated into 129Sv embryonic stem (ES) cells. G418 and gancyclovir resistant clones were analyzed by Southern blot. The correct targeted ES cell lines were expanded and injected into blastocysts. PCR analyses were performed to confirm the inclusion of distal *loxP* site before blastocyst injection. Male chimeras were bred to C57BL/6J females to generate F1 offspring. The *Jup* floxed mice were maintained in a mixed 129Sv-C57BL/6J genetic background. The floxed mice were genotyped by PCR using the following primers: JupF, 5′-AAAGCCTACAGCAGC ATCGT-3′; JupR, 5′-CCCCTTCCCTCTTTTCATCT-3′. The neomycin cassette was selectively removed by breeding to *EIIa-Cre* mice (50). Southern blot and PCR confirmed the expected homologous recombination event and germ-line transmission of the targeted allele (Fig. 1B and C).

All protocols involving the use of animals were in compliance with the National Institutes of Health's and the Indiana University Laboratory Animals Research Committee's Guide for the Care and Use of Laboratory Animals. *EIIa* transgenic *Cre* mice, *αMHC* transgenic *Cre* mice, and *Fos-lacZ* transgenic *Cre* mice were purchased from The Jackson laboratory.

Southern blot

After digestion with *Nsi*I, the DNA fragments were separated by electrophoresis in 0.7% agarose gels and transferred to Hybond-N+ membranes. ^{32}P-labeled probes were made using the multiprime-labeling system (Amersham). The labeling DNA template (size: 360 bp) was generated by PCR using one pair of primers: forward, 5′-CACACCGGAGCTCATT AACA-3′; reverse, 5′-CCTTCAAAACTACTTCCTCACC AT-3′. Hybridizations were carried out at 60°C overnight in hybridization buffer.

Quantitative RT–PCR

Total RNA was extracted from hearts using Trizol reagent (Invitrogen). SYBR green qRT-PCR analyses were performed

using Roche LightCycler 480. Primers are listed in Supplementary Material, Table S7.

Immunoblot analysis

Hearts were lysed with radioimmunoprecipitation assay buffer. Proteins were resolved in 4–12% Bis–Tris gels and subsequently transferred and immunoblotted. Antibodies used were: polyclonal antibody (pAb) against Jup, N-Cadherin, Bcl-2, Bax, Smad1, Smad2 (Santa Cruz Biotechnology); mAb against α-catenin (Santa Cruz Biotechnology); pAb against β-Catenin, phospho-JNK (Thr183/Tyr185), total-JNK, phosphor-P38MAPK, P38MAPK, phosphor-Smad1 (ser463/465), Caspase-8, cleaved Caspase-3 and PARP (Cell Signaling Technology); pAb against phosphor-Smad2 (Ser465/467) (Millipore); mAb again Rac1 (Upstate); mAb against sarcomeric α-actinin (Sigma). pAb against Nix (Abcam). mAb against Desmoglein 1+2 (Progen).

Immunostaining

For immunofluorescence staining, fluorophore-conjugated wheat germ agglutinin (WGA) and Alexa Fluor secondary antibodies were purchased from Molecular Probes. Nuclei were stained with 4′,6-diamidino-2-phenylindole (DAPI). Immunohistochemical (IHC) stainings were performed using Vectastain ABC kits (Vector Labs) and counterstained by hematoxylin. Slides were treated for epitope retrieval prior to IHC stainings. Photomicrographs were acquired with a Leica microscope using a single photographing condition for the same set of sections for each staining. Antibodies: Gr-1 and F4/80 (BD pharmingen), Ki67 and CyclinD 1 (Vector labs) and TGFβ1 (Santa Cruz Biotechnology).

Masson's trichrome staining, Sirius red-fast green staining and Yasue staining

The stainings were carried out as described previously (51).

TUNEL assay

TUNEL assays were performed on paraffin sections by using the Apoptag kit (Chemicon, Temecula, CA, USA). The assays were conducted according to the protocol recommended by the manufacturer. The cell death signal displays green fluorescence as the antibody is conjugated with fluorescein isothiocyanate (FITC). Percentage of positively stained cardiomyocytes was quantified by counting of FITC-stained cardiomyocytes out of total DAPI-stained cardiomyocytes in each photograph. On average, eight photographs were randomly taken for each sample.

EBD injection

EBD injection was performed as previously described (25). Briefly, 18-day-old mice were injected intraperitoneally with EBD (0.5 mg EBD/0.1 ml phosphate buffered saline (PBS)/10 g body weight). Injected mice were returned to their cages with food and water *ad libitum*. After 24 h, mice were sacrificed and hearts were harvested for cryosections. EBD displays red auto-fluorescence under a fluorescence microscope.

Echocardiographic analyses

Transthoracic echocardiograms were performed on mice under 1.5–2% isoflurane anesthesia as described previously (52).

Electrophysiologic and optical mapping study

Surface ECG recording was performed as previously described (53). Mice were anesthetized with 4% isoflurane before placing the electrodes and the anesthesia was maintained with 2% isoflurane through a nose cone. The isolated hearts were perfused using a Langendorf perfusion system with 37°C Tyrode's solution. The heart was immersed in a water-jacketed bath and maintained at 37°C. A global ECG was recorded through bath solution. A 2Fr octapolar electrode catheter with 0.5 mm interelectrode distance (NuMed Inc., Hopkinton, NY, USA) was used to record intracardiac bipolar electrograms from the RA and RV and also used for pacing (RV apex, output: twice diastolic threshold). Burst ventricular pacing (up to the minimal pacing cycle length with 1:1 capture) or ventricular extrastimuli (S1: 10 beats, two different cycle lengths; S2–S4 with progressively decreasing coupling intervals) was performed to determine the inducibility of VTs.

Optical mapping study was carried out as described previously (53).

Transmission electron microscopy

Heart samples were fixed in modified Karnovskv's buffer (2% paraformaldehyde/2% glutaraldehyde in 0.1 M phosphate buffer) at 4°C overnight. On the next day, the specimens were post-fixed in 1% osmium tetroxide in PBS for 1 h at room temperature. Then the samples were further dehydrated by a series of graded ethanol and embedded for sectioning. Digital pictures were taken with a Tecnai G212 Bio Twin TEM microscope (Hillsboro, OR, USA), equipped with an AMT CCD Camera (Danvers, MA, USA).

Statistical analysis

Results were expressed as mean ± SEM for parametric data. Student's *t*-test was performed for comparison between the two groups of parametric data. χ^2-test was applied for the analysis of ratios of different genotypes versus theoretical Mendelian ratios. *P*-values of <0.05 were considered significant.

SUPPLEMENTARY MATERIAL

Supplementary Material is available at *HMG* online.

ACKNOWLEDGEMENTS

We thank Dr Michael Rubart (IU, Indianapolis) for generously providing us with Connexin43 Ab.

Conflict of Interest statement. None declared.

FUNDING

This work was supported, in whole or in part, by National Institutes of Health (W.S., L.J.F. and P.S.C.) and a Medtronic-Zipes Endowment (P.S.C.).

REFERENCES

1. Basso, C., Corrado, D., Marcus, F.I., Nava, A. and Thiene, G. (2009) Arrhythmogenic right ventricular cardiomyopathy. *Lancet*, **373**, 1289–1300.
2. Lahtinen, A.M., Lehtonen, E., Marjamaa, A., Kaartinen, M., Helio, T., Porthan, K., Oikarinen, L., Toivonen, L., Swan, H., Jula, A. *et al.* (2011) Population-prevalent desmosomal mutations predisposing to arrhythmogenic right ventricular cardiomyopathy. *Heart Rhythm*, **8**, 1214–1221.
3. Maron, B.J., Shirani, J., Poliac, L.C., Mathenge, R., Roberts, W.C. and Mueller, F.O. (1996) Sudden death in young competitive athletes. Clinical, demographic, and pathological profiles. *J. Am. Med. Assoc.*, **276**, 199–204.
4. Protonotarios, N.I., Tsatsopoulou, A.A. and Gatzoulis, K.A. (2002) Arrhythmogenic right ventricular cardiomyopathy caused by a deletion in plakoglobin (Naxos disease). *Card. Electrophysiol. Rev.*, **6**, 72–80.
5. Lai-Cheong, J.E., Arita, K. and McGrath, J.A. (2007) Genetic diseases of junctions. *J. Invest. Dermatol.*, **127**, 2713–2725.
6. Beffagna, G., Occhi, G., Nava, A., Vitiello, L., Ditadi, A., Basso, C., Bauce, B., Carraro, G., Thiene, G., Towbin, J.A. *et al.* (2005) Regulatory mutations in transforming growth factor-beta3 gene cause arrhythmogenic right ventricular cardiomyopathy type 1. *Cardiovasc. Res.*, **65**, 366–373.
7. den Haan, A.D., Tan, B.Y., Zikusoka, M.N., Llado, L.I., Jain, R., Daly, A., Tichnell, C., James, C., Amat-Alarcon, N., Abraham, T. *et al.* (2009) Comprehensive desmosome mutation analysis in north americans with arrhythmogenic right ventricular dysplasia/cardiomyopathy. *Circ. Cardiovasc. Genet.*, **2**, 428–435.
8. Green, K.J. and Gaudry, C.A. (2000) Are desmosomes more than tethers for intermediate filaments? *Nat. Rev. Mol. Cell Biol.*, **1**, 208–216.
9. Garcia-Gras, E., Lombardi, R., Giocondo, M.J., Willerson, J.T., Schneider, M.D., Khoury, D.S. and Marian, A.J. (2006) Suppression of canonical Wnt/beta-catenin signaling by nuclear plakoglobin recapitulates phenotype of arrhythmogenic right ventricular cardiomyopathy. *J. Clin. Invest.*, **116**, 2012–2021.
10. Pilichou, K., Remme, C.A., Basso, C., Campian, M.E., Rizzo, S., Barnett, P., Scicluna, B.P., Bauce, B., van den Hoff, M.J., de Bakker, J.M. *et al.* (2009) Myocyte necrosis underlies progressive myocardial dystrophy in mouse dsg2-related arrhythmogenic right ventricular cardiomyopathy. *J. Exp. Med.*, **206**, 1787–1802.
11. Yang, Z., Bowles, N.E., Scherer, S.E., Taylor, M.D., Kearney, D.L., Ge, S., Nadvoretskiy, V.V., DeFreitas, G., Carabello, B., Brandon, L.I. *et al.* (2006) Desmosomal dysfunction due to mutations in desmoplakin causes arrhythmogenic right ventricular dysplasia/cardiomyopathy. *Circ. Res.*, **99**, 646–655.
12. McKoy, G., Protonotarios, N., Crosby, A., Tsatsopoulou, A., Anastasakis, A., Coonar, A., Norman, M., Baboonian, C., Jeffery, S. and McKenna, W.J. (2000) Identification of a deletion in plakoglobin in arrhythmogenic right ventricular cardiomyopathy with palmoplantar keratoderma and woolly hair (Naxos disease). *Lancet*, **355**, 2119–2124.
13. Kirchhof, P., Fabritz, L., Zwiener, M., Witt, H., Schafers, M., Zellerhoff, S., Paul, M., Athai, T., Hiller, K.H., Baba, H.A. *et al.* (2006) Age- and training-dependent development of arrhythmogenic right ventricular cardiomyopathy in heterozygous plakoglobin-deficient mice. *Circulation*, **114**, 1799–1806.
14. Agah, R., Frenkel, P.A., French, B.A., Michael, L.H., Overbeek, P.A. and Schneider, M.D. (1997) Gene recombination in postmitotic cells. Targeted expression of Cre recombinase provokes cardiac-restricted, site-specific rearrangement in adult ventricular muscle in vivo. *J. Clin. Invest.*, **100**, 169–179.
15. MacLellan, W.R., Garcia, A., Oh, H., Frenkel, P., Jordan, M.C., Roos, K.P. and Schneider, M.D. (2005) Overlapping roles of pocket proteins in the myocardium are unmasked by germ line deletion of p130 plus heart-specific deletion of Rb. *Mol. Cell Biol.*, **25**, 2486–2497.
16. Basso, C., Thiene, G., Corrado, D., Angelini, A., Nava, A. and Valente, M. (1996) Arrhythmogenic right ventricular cardiomyopathy. Dysplasia, dystrophy, or myocarditis? *Circulation*, **94**, 983–991.
17. Kaplan, S.R., Gard, J.J., Protonotarios, N., Tsatsopoulou, A., Spiliopoulou, C., Anastasakis, A., Squarcioni, C.P., McKenna, W.J., Thiene, G., Basso, C. *et al.* (2004) Remodeling of myocyte gap junctions in arrhythmogenic right ventricular cardiomyopathy due to a deletion in plakoglobin (Naxos disease). *Heart Rhythm*, **1**, 3–11.
18. Hamilton, R.M. (2009) Arrhythmogenic right ventricular cardiomyopathy. *Pacing Clin. Electrophysiol.*, **32**(Suppl. 2), S44–51.
19. Zhurinsky, J., Shtutman, M. and Ben-Ze'ev, A. (2000) Plakoglobin and beta-catenin: protein interactions, regulation and biological roles. *J. Cell Sci.*, **113**(Pt 18), 3127–3139.
20. Bierkamp, C., Schwarz, H., Huber, O. and Kemler, R. (1999) Desmosomal localization of beta-catenin in the skin of plakoglobin null-mutant mice. *Development*, **126**, 371–381.
21. Soonpaa, M.H., Koh, G.Y., Pajak, L., Jing, S., Wang, H., Franklin, M.T., Kim, K.K. and Field, L.J. (1997) Cyclin D1 overexpression promotes cardiomyocyte DNA synthesis and multinucleation in transgenic mice. *J. Clin. Invest.*, **99**, 2644–2654.
22. DasGupta, R. and Fuchs, E. (1999) Multiple roles for activated LEF/TCF transcription complexes during hair follicle development and differentiation. *Development*, **126**, 4557–4568.
23. Grasl-Kraupp, B., Ruttkay-Nedecky, B., Koudelka, H., Bukowska, K., Bursch, W. and Schulte-Hermann, R. (1995) In situ detection of fragmented DNA (TUNEL assay) fails to discriminate among apoptosis, necrosis, and autolytic cell death: a cautionary note. *Hepatology*, **21**, 1465–1468.
24. Thomsen, H. and Held, H. (1994) Susceptibility of C5b-9(m) to postmortem changes. *Int. J. Legal Med.*, **106**, 291–293.
25. Han, R., Bansal, D., Miyake, K., Muniz, V.P., Weiss, R.M., McNeil, P.L. and Campbell, K.P. (2007) Dysferlin-mediated membrane repair protects the heart from stress-induced left ventricular injury. *J. Clin. Invest.*, **117**, 1805–1813.
26. Chen, G. and Goeddel, D.V. (2002) TNF-R1 signaling: a beautiful pathway. *Science*, **296**, 1634–1635.
27. Kitsis, R.N. and Molkentin, J.D. (2010) Apoptotic cell death 'Nixed' by an ER-mitochondrial necrotic pathway. *Proc. Natl Acad. Sci. USA*, **107**, 9031–9032.
28. Dhanasekaran, D.N. and Reddy, E.P. (2008) JNK signaling in apoptosis. *Oncogene*, **27**, 6245–6251.
29. Heldin, C.H., Landstrom, M. and Moustakas, A. (2009) Mechanism of TGF-beta signaling to growth arrest, apoptosis, and epithelial-mesenchymal transition. *Curr. Opin. Cell Biol.*, **21**, 166–176.
30. Kania, G., Blyszczuk, P. and Eriksson, U. (2009) Mechanisms of cardiac fibrosis in inflammatory heart disease. *Trends Cardiovasc. Med.*, **19**, 247–252.
31. Chen, H., Yong, W., Ren, S., Shen, W., He, Y., Cox, K.A., Zhu, W., Li, W., Soonpaa, M., Payne, R.M. *et al.* (2006) Overexpression of bone morphogenetic protein 10 in myocardium disrupts cardiac postnatal hypertrophic growth. *J. Biol. Chem.*, **281**, 27481–27491.
32. Ranganathan, P., Agrawal, A., Bhushan, R., Chavalmane, A.K., Kalathur, R.K., Takahashi, T. and Kondaiah, P. (2007) Expression profiling of genes regulated by TGF-beta: differential regulation in normal and tumour cells. *BMC Genomics*, **8**, 98.
33. Khalil, N. (1999) TGF-beta: from latent to active. *Microbes Infect.*, **1**, 1255–1263.
34. Kassiri, Z., Defamie, V., Hariri, M., Oudit, G.Y., Anthwal, S., Dawood, F., Liu, P. and Khokha, R. (2009) Simultaneous transforming growth factor beta-tumor necrosis factor activation and cross-talk cause aberrant remodeling response and myocardial fibrosis in Timp3-deficient heart. *J. Biol. Chem.*, **284**, 29893–29904.
35. Christensen, A.H., Benn, M., Bundgaard, H., Tybjaerg-Hansen, A., Haunso, S. and Svendsen, J.H. (2010) Wide spectrum of desmosomal mutations in Danish patients with arrhythmogenic right ventricular cardiomyopathy. *J. Med. Genet.*, **47**, 736–744.
36. Sen-Chowdhry, S., Morgan, R.D., Chambers, J.C. and McKenna, W.J. (2010) Arrhythmogenic cardiomyopathy: etiology, diagnosis, and treatment. *Annu. Rev. Med.*, **61**, 233–253.
37. Sen-Chowdhry, S., Lowe, M.D., Sporton, S.C. and McKenna, W.J. (2004) Arrhythmogenic right ventricular cardiomyopathy: clinical presentation, diagnosis, and management. *Am. J. Med.*, **117**, 685–695.

38. Basso, C., Czarnowska, E., Della Barbera, M., Bauce, B., Beffagna, G., Wlodarska, E.K., Pilichou, K., Ramondo, A., Lorenzon, A., Wozniek, O. *et al.* (2006) Ultrastructural evidence of intercalated disc remodelling in arrhythmogenic right ventricular cardiomyopathy: an electron microscopy investigation on endomyocardial biopsies. *Eur. Heart J.*, **27**, 1847–1854.
39. Li, J., Swope, D., Raess, N., Cheng, L., Muller, E.J. and Radice, G.L. (2011) Cardiac tissue-restricted deletion of plakoglobin results in progressive cardiomyopathy and activation of {beta}-catenin signaling. *Mol. Cell Biol.*, **31**, 1134–1144.
40. Matsuo, S., Sato, Y., Nakae, I., Masuda, D., Yomota, M., Ashihara, T. and Horie, M. (2007) Left ventricular involvement in arrhythmogenic right ventricular cardiomyopathy demonstrated by multidetector-row computed tomography. *Int. J. Cardiol.*, **115**, e129–131.
41. Mackey-Bojack, S.M., Roe, S.J. and Titus, J.L. (2009) Sudden death with circumferential subepicardial fibrofatty replacement: left-sided arrhythmogenic ventricular cardiomyopathy. *Am. J. Forensic. Med. Pathol.*, **30**, 209–214.
42. Sen-Chowdhry, S., Syrris, P., Prasad, S.K., Hughes, S.E., Merrifield, R., Ward, D., Pennell, D.J. and McKenna, W.J. (2008) Left-dominant arrhythmogenic cardiomyopathy: an under-recognized clinical entity. *J. Am. Coll. Cardiol.*, **52**, 2175–2187.
43. McCauley, M.D. and Wehrens, X.H. (2009) Animal models of arrhythmogenic cardiomyopathy. *Dis. Model. Mech.*, **2**, 563–570.
44. Chen, X., Shevtsov, S.P., Hsich, E., Cui, L., Haq, S., Aronovitz, M., Kerkela, R., Molkentin, J.D., Liao, R., Salomon, R.N. *et al.* (2006) The beta-catenin/T-cell factor/lymphocyte enhancer factor signaling pathway is required for normal and stress-induced cardiac hypertrophy. *Mol. Cell Biol.*, **26**, 4462–4473.
45. Baurand, A., Zelarayan, L., Betney, R., Gehrke, C., Dunger, S., Noack, C., Busjahn, A., Huelsken, J., Taketo, M.M., Birchmeier, W. *et al.* (2007) Beta-catenin downregulation is required for adaptive cardiac remodeling. *Circ. Res.*, **100**, 1353–1362.
46. Mallat, Z., Tedgui, A., Fontaliran, F., Frank, R., Durigon, M. and Fontaine, G. (1996) Evidence of apoptosis in arrhythmogenic right ventricular dysplasia. *N. Engl. J. Med.*, **335**, 1190–1196.
47. McLennan, I.S. and Koishi, K. (2002) The transforming growth factor-betas: multifaceted regulators of the development and maintenance of skeletal muscles, motoneurons and Schwann cells. *Int. J. Dev. Biol.*, **46**, 559–567.
48. Taniguti, A.P., Pertille, A., Matsumura, C.Y., Santo Neto, H. and Marques, M.J. (2011) Prevention of muscle fibrosis and myonecrosis in mdx mice by suramin, a TGF-beta1 blocker. *Muscle Nerve*, **43**, 82–87.
49. Buja, L.M. and Vela, D. (2008) Cardiomyocyte death and renewal in the normal and diseased heart. *Cardiovasc. Pathol.*, **17**, 349–374.
50. Lakso, M., Pichel, J.G., Gorman, J.R., Sauer, B., Okamoto, Y., Lee, E., Alt, F.W. and Westphal, H. (1996) Efficient in vivo manipulation of mouse genomic sequences at the zygote stage. *Proc. Natl Acad. Sci. USA*, **93**, 5860–5865.
51. Pasumarthi, K.B., Nakajima, H., Nakajima, H.O., Soonpaa, M.H. and Field, L.J. (2005) Targeted expression of cyclin D2 results in cardiomyocyte DNA synthesis and infarct regression in transgenic mice. *Circ. Res.*, **96**, 110–118.
52. Li, D., Hallett, M.A., Zhu, W., Rubart, M., Liu, Y., Yang, Z., Chen, H., Haneline, L.S., Chan, R.J., Schwartz, R.J. *et al.* (2011) Dishevelled-associated activator of morphogenesis 1 (Daam1) is required for heart morphogenesis. *Development*, **138**, 303–315.
53. Maruyama, M., Li, B.Y., Chen, H., Xu, X., Song, L.S., Guatimosim, S., Zhu, W., Yong, W., Zhang, W., Bu, G. *et al.* (2011) FKBP12 is a critical regulator of the heart rhythm and the cardiac voltage-gated sodium current in mice. *Circ. Res.*, **108**, 1042–1052.